19. X. G. Peralta *et al.*, *Opt. Express* **17**, 773 (2009).
20. A. C. Strikwerda *et al.*, *Opt. Express* **17**, 136 (2009).
21. Y. J. Chiang, T. J. Yen, *Appl. Phys. Lett.* **102**, 011129 (2013).
22. N. F. Yu *et al.*, *Science* **334**, 333 (2011).
23. X. J. Ni, N. K. Emani, A. V. Kildishev, A. Boltasseva, V. M. Shalaev, *Science* **335**, 427 (2012).
24. H.-T. Chen *et al.*, *Phys. Rev. Lett.* **105**, 073901 (2010).
25. H.-T. Chen, *Opt. Express* **20**, 7165 (2012).
26. Materials and methods are available as supplementary materials on *Science* Online.
27. S. L. Sun *et al.*, *Nat. Mater.* **11**, 426 (2012).
28. S. Franke-Arnold, L. Allen, M. Padgett, *Laser Photon. Rev.* **2**, 299 (2008).
29. R. Fickler *et al.*, *Science* **338**, 640 (2012).
30. J. Wang *et al.*, *Nat. Photonics* **6**, 488 (2012).

Acknowledgments: We acknowledge partial support from the Los Alamos National Laboratory Laboratory-Directed Research and Development program. This work was performed in part at the Center for Integrated Nanotechnologies, a U.S. Department of Energy, Office of Basic Energy Sciences user facility. Los Alamos National Laboratory, an affirmative action equal opportunity employer, is operated by Los Alamos National Security for the National Nuclear Security Administration of the U.S. Department of Energy under contract DE-AC52-06NA25396.

Supplementary Materials
www.sciencemag.org/cgi/content/full/science.1235399/DC1
Materials and Methods
Figs. S1 to S8
References (*31*–*35*)

21 January 2013; accepted 1 May 2013
Published online 16 May 2013;
10.1126/science.1235399

Short-Range Quantum Magnetism of Ultracold Fermions in an Optical Lattice

Daniel Greif,[1] Thomas Uehlinger,[1] Gregor Jotzu,[1] Leticia Tarruell,[1,2]* Tilman Esslinger[1]†

Quantum magnetism originates from the exchange coupling between quantum mechanical spins. Here, we report on the observation of nearest-neighbor magnetic correlations emerging in the many-body state of a thermalized Fermi gas in an optical lattice. The key to obtaining short-range magnetic order is a local redistribution of entropy, which allows temperatures below the exchange energy for a subset of lattice bonds. When loading a repulsively interacting gas into either dimerized or anisotropic simple cubic configurations of a tunable-geometry lattice, we observe an excess of singlets as compared with triplets consisting of two opposite spins. For the anisotropic lattice, the transverse spin correlator reveals antiferromagnetic correlations along one spatial axis. Our work facilitates addressing open problems in quantum magnetism through the use of quantum simulation.

Quantum magnetism describes quantum many-body states of spins coupled by exchange interactions and lies at the heart of many fundamental phenomena in condensed matter physics (*1*, *2*). Spin systems often tend to show long-range order at low temperatures; however, the interplay of exchange interactions with geometry and quantum fluctuations can lead to quantum states characterized by their short-range magnetic order. Examples include valence-bond crystals, spin-liquids, and possibly high-temperature superconductors (*1*–*5*). Interestingly, the underlying many-body physics gives rise to computationally and theoretically intractable regimes, even in the phase diagrams of simple models such as the Fermi-Hubbard model. Moreover, the direct measurement of local spin correlations in solids remains a major challenge.

The controlled setting of ultracold fermionic atoms in optical lattices is regarded as a promising route to gain new insights into phases driven by quantum magnetism (*6*–*8*). This approach offers experimental access to a clean and highly flexible Fermi-Hubbard model with a distinct set of observables (*9*). For repulsively interacting fermions, density ordering in the metal–Mott insulator transition has been explored experimentally (*10*, *11*). Yet, progress toward entering the regime of quantum magnetism has been hindered by the ultralow temperatures and entropies required to observe exchange-driven spin ordering in optical lattices. For bosonic systems, promising progress has been reported: By mapping the spin onto the site occupation or the local phase of a Bose-Einstein condensate, the physics of one-dimensional (1D) decoupled Ising spin chains (*12*) and classical magnetism on a triangular lattice could be simulated (*13*). Furthermore, arrays of isolated double wells and plaquettes were used to study the exchange dynamics of artificially prepared few-boson systems (*14*, *15*).

To enable the study of quantum magnetic phenomena in thermalized many-body Hubbard systems, cooling schemes based on the redistribution of entropy between different regions of the trap have been suggested (*16*, *17*). In this work, we propose and implement a local entropy-redistribution scheme within the lattice structure to reach the regime of quantum magnetism. The atoms are either prepared in a dimerized or an anisotropic simple cubic lattice (Fig. 1). In both geometries, a subset of links of the underlying simple cubic lattice is set to a larger exchange energy as compared with the other links. As a result, the entropy is predominantly stored in configurations involving the weak links. For fixed total entropy in the trapped system, this allows us to reach temperatures between the two exchange-energy scales.

The experiment is performed with a harmonically confined, balanced two-component mixture of a quantum degenerate Fermi gas of ^{40}K. The atoms are prepared in two magnetic sublevels, $m_F = -9/2$ and $-7/2$, of the $F = 9/2$ hyperfine manifold, denoted by ↑ and ↓, at temperatures below 10% of the Fermi temperature. We load 50,000 to 100,000 repulsively interacting atoms at an s-wave scattering length of $106(1)a_0$ into the 3D optical lattice, where a_0 denotes the Bohr radius. The lattice is created by a combination of interfering laser beams

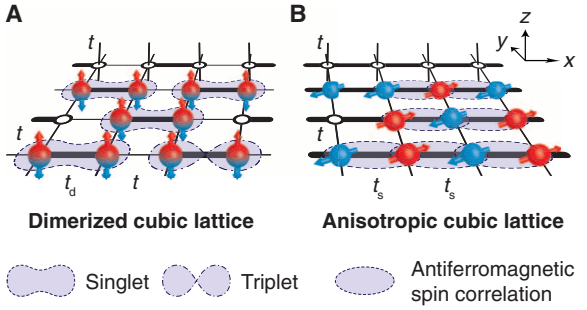

Fig. 1. Magnetic spin correlations. Schematic view of the nearest-neighbor spin correlations observed in the experiment. A two-component mixture of fermionic atoms (red and blue) is prepared close to half-filling in a cubic lattice with two different tunnel-coupling configurations. (**A**) Dimerized lattice with the strong dimer links t_d and weaker links t. Low temperatures lead to an excess number of singlets over triplets. (**B**) Anisotropic lattice with strong and weak tunneling t_s and t along different spatial axes. Antiferromagnetic spin correlations in the transverse direction are formed along the strong-link direction. In both panels, exemplary thermal excitations in the form of spin excitations, or holes, are shown.

[1]Institute for Quantum Electronics, ETH Zurich, 8093 Zurich, Switzerland. [2]LP2N UMR 5298, Université Bordeaux 1, Institut d'Optique and CNRS, 351 Cours de la Libération, 33405 Talence, France.

*Present address: Institut de Ciencies Fotoniques, Mediterranean Technology Park, 08860 Castelldefels, Barcelona, Spain. †Corresponding author. E-mail: esslinger@phys.ethz.ch

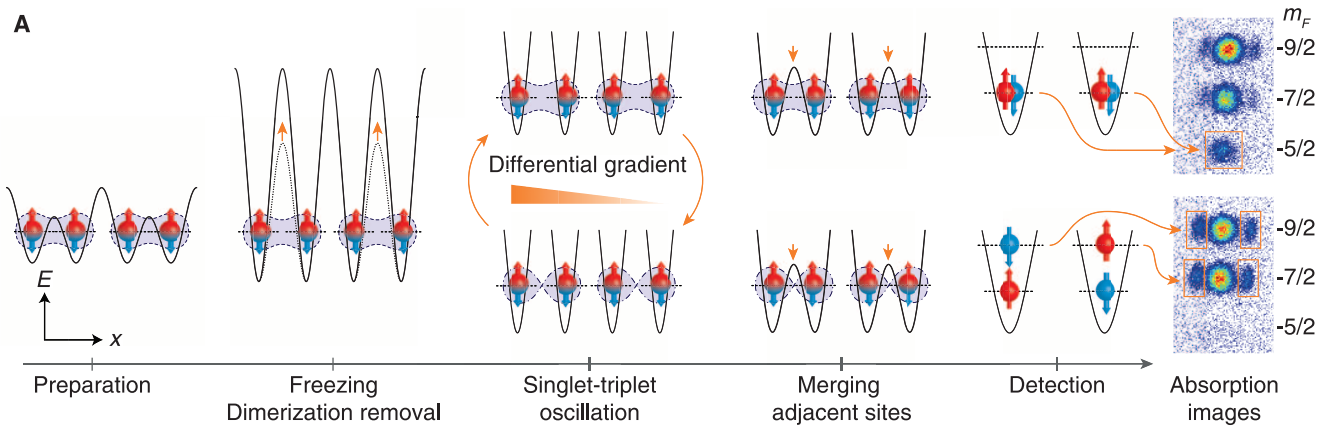

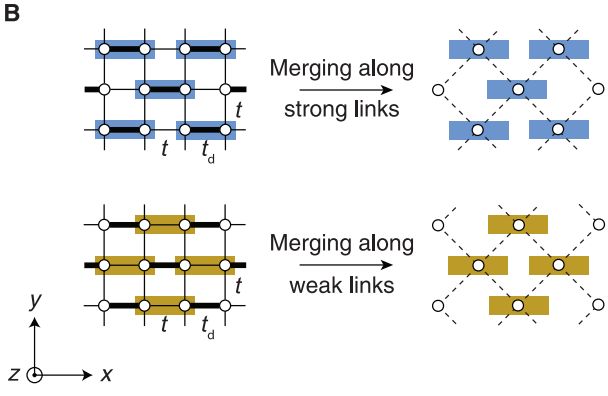

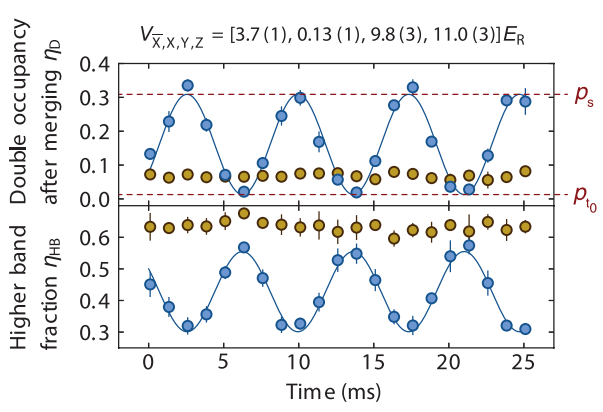

Fig. 2. Detection scheme for singlets and triplets. (**A**) Schematics of the detection steps for the case of two singlets in a dimerized lattice. Depending on the oscillation time, the absorption images on the right show either a large double occupancy in the lowest band, corresponding to singlets (top row), or an increased higher-band fraction, indicating triplet states (bottom row). (**B**) The two possible merging configurations in a dimerized lattice. Singlets and triplets are detected on a set of adjacent sites arranged on a checkerboard pattern in the plane. (**C**) Singlet-triplet oscillation in a strongly dimerized lattice with U/t = 10.9(8) and t_d/t = 20(2). We observe oscillations in the double occupancy after merging, η_D, and in the higher-band fraction, η_{HB}, when merging along the strong links (blue), whereas no oscillations are visible for the weak links (ocher). The phase of the oscillation is shifted, owing to the double-occupancy–removal procedure (*20*). The red dashed lines denote the extracted singlet and triplet fractions, p_s and p_{t_0}, respectively. Error bars indicate SD of at least five measurements.

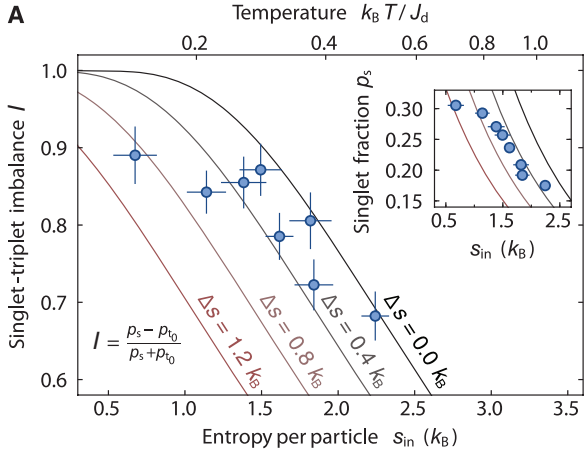

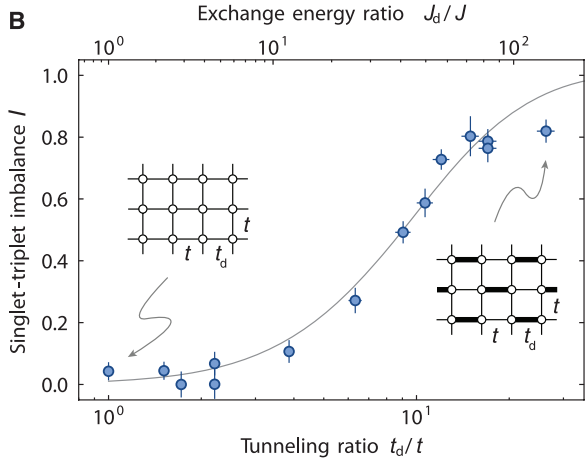

Fig. 3. Dimerized simple cubic lattice. (**A**) Singlet-triplet imbalance on the strong dimer links versus initial entropy before loading into the lattice (s_{in}) and temperature (k_BT/J_d) in a dimerized lattice with U/t = 10.9(8) and t_d/t = 20(2), where t/h = 67(6) Hz. This corresponds to an exchange-energy ratio of J_d/J = 100(9), with J/h = 24(2) Hz. The imbalance and absolute singlet fraction (inset) decrease with increasing entropy. Solid curves show the prediction of a high-temperature series expansion, taking into account different amounts of added entropy Δs during the lattice loading. (**B**) Imbalance versus dimerization t_d/t and J_d/J, showing an increase for strongly dimerized simple cubic lattices. As the dimerization is increased, the exchange energy J/h increases from 18(3) to 27(3) Hz, because U/t is reduced (*20*). The solid curve shows the theory prediction for an entropy per particle of 1.7k_B in the lattice, which includes the heating during loading. Vertical error bars denote the fit error from singlet-triplet oscillations consisting of 63 measurements, the errors in t_d/t stem from lattice calibration uncertainties, and the errors in s_{in} are the SD of five measurements. Individual curves of p_s and p_{t_0} for all measurements are shown in (*20*).

operating at a wavelength λ = 1064 nm with lattice depths $V_{\bar{X}}$, V_X, V_Y, and V_Z, which are given in units of recoil energy $E_R = h^2/2m\lambda^2$ (*18*–*20*). Here, m denotes the mass of ^{40}K and h is Planck's constant. We independently control the tunneling strengths along all three spatial axes. In addition, we can introduce a checkerboard dimerization in the xy plane by strengthening every second tunneling link along the x axis (Fig. 1A). The checkerboard pattern is replicated along the z axis. Our system is well described by a 3D single-band Hubbard model with repulsive on-site interaction energy U, unless explicitly stated. The tunneling t along the weak links in both lattice geometries is set to $t/h = 67(6)$ Hz for all measurements. The strong tunneling is denoted by t_d and t_s in the dimerized and anisotropic lattice, respectively.

As shown in Fig. 2, A and B, the fraction of atoms forming singlets (p_s) and triplets (p_{t_0}) on neighboring lattice sites is detected by transforming the lattice to a checkerboard geometry, similar to a previously developed technique (*21*). The first part of our detection sequence consists of freezing out the atomic motion. In the anisotropic lattice, we perform a sudden ramp into a deep, simple cubic structure with negligible tunneling. The final singlet measurement then corresponds to projecting pairs of sites onto $|s\rangle = |\uparrow,\downarrow\rangle - |\downarrow,\uparrow\rangle/\sqrt{2}$. In the dimerized lattice, we apply a two-step ramp, such that the final singlet measurement locally projects onto the singlet eigenstate of an isolated pair of sites (*20*). There, the intensity of all lattice beams is ramped up proportionally, before the lattice is adiabatically transformed into a simple cubic configuration. For both lattice geometries, the final triplet measurement projects pairs of sites onto $|t_0\rangle = |\uparrow,\downarrow\rangle + |\downarrow,\uparrow\rangle/\sqrt{2}$. In the deep cubic lattice, all atoms on doubly occupied sites are removed. We then apply a magnetic field gradient, which creates a differential bias energy Δ for atoms of opposite spins on adjacent sites and causes coherent oscillations between the singlet $|s\rangle$ and triplet $|t_0\rangle$ states at a frequency $\nu = \Delta/h$. If the initial amount of singlets and triplets is equal, no overall oscillation will be visible, as $|s\rangle$ and $|t_0\rangle$ oscillate in antiphase.

After a certain oscillation time, we remove the gradient and merge pairs of adjacent sites. Owing to the symmetry of the two-particle wave function, the singlet state on neighboring sites evolves to a doubly occupied site with both atoms in the lowest band, whereas the triplet state transforms into a state with one atom in the lowest and one atom in the first excited band. The fraction of atoms forming double occupancies in the lowest band of the merged lattice, η_D, is detected by an interaction-dependent radiofrequency transfer to the previously unpopulated $m_F = -5/2$ spin state (*10*). The fraction of atoms in the higher band, η_{HB}, is obtained from a band-mapping technique (*8*). For the final readout, we take absorption images after Stern-Gerlach separation of the spin states during ballistic expansion. For an imbalance between the initial singlet and triplet populations, η_D and η_{HB} will show oscillations with opposite amplitudes. As the double occupancy in the lowest band contains only contributions from two particles with opposite spins, we can infer the fraction of atoms forming singlets and triplets from the maxima and minima of a sinusoidal fit to η_D. The higher-band fraction has an additional offset caused by dimers containing two atoms with the same spin or one atom with an antisymmetric spatial wave function.

When loading atoms into a strongly dimerized lattice and merging along the strong links, we observe oscillations in η_D and η_{HB} (Fig. 2C). This reveals an excess number of singlets, corresponding to magnetic order on neighboring sites. We quantify this order by the normalized imbalance

$$I = \frac{p_s - p_{t_0}}{p_s + p_{t_0}} \quad (1)$$

The order in the strongly dimerized lattice originates from temperatures below the intradimer exchange energy $J_d = -U/2 + \sqrt{16t_d^2 + U^2}/2$, which denotes the singlet-triplet splitting on a single dimer. Although such temperatures require very low entropies for isotropic lattices (*22*), in our system the access to the regime of magnetic ordering is facilitated by the presence of the weaker interdimer exchange energy $J \ll J_d$. This leads to an entropy redistribution from states on the strong to the weak links and gives access to the temperature regime $J < k_B T < J_d$ for experimentally attainable entropies (here, k_B denotes the Boltzmann constant and T is temperature). As expected for strong dimerizations, we find no visible oscillations when merging along the weak links, which indicates the absence of magnetic correlations on these links (Fig. 2C). We measure constant values of $\eta_D = 0.07(1)$ and $\eta_{HB} = 0.63(3)$, which are consistent with a state in which nearly all singlets are located on neighboring dimer links, with vanishing correlations between them. The observed correlation pattern

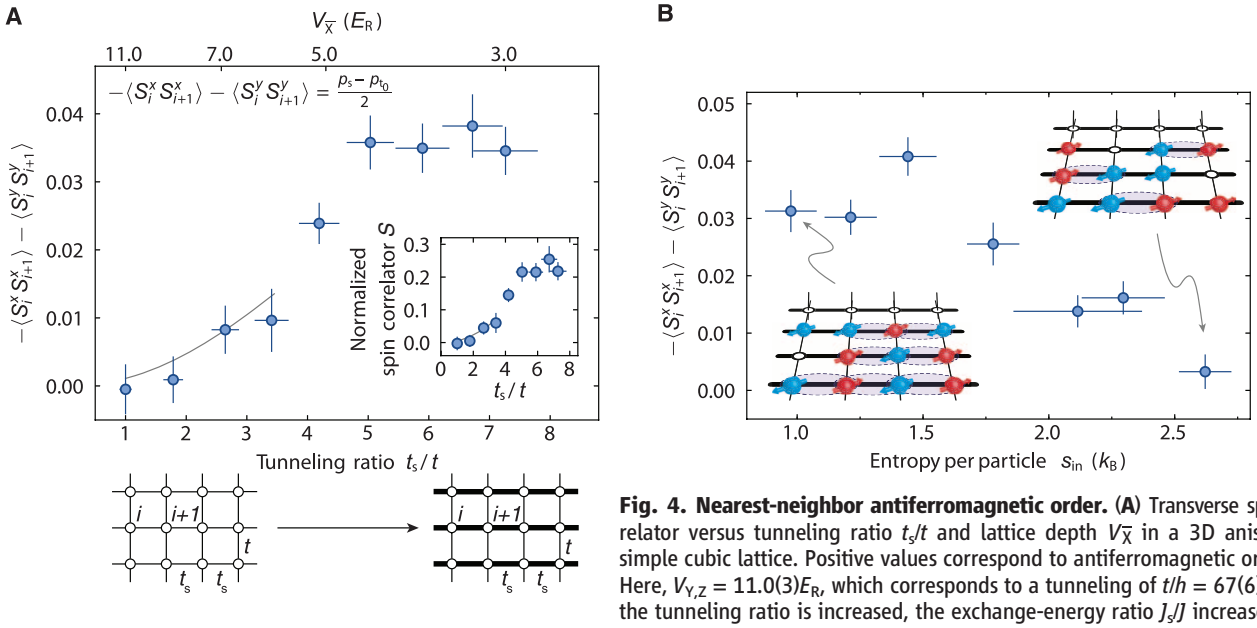

Fig. 4. Nearest-neighbor antiferromagnetic order. (**A**) Transverse spin correlator versus tunneling ratio t_s/t and lattice depth $V_{\bar{X}}$ in a 3D anisotropic simple cubic lattice. Positive values correspond to antiferromagnetic ordering. Here, $V_{Y,Z} = 11.0(3)E_R$, which corresponds to a tunneling of $t/h = 67(6)$ Hz. As the tunneling ratio is increased, the exchange-energy ratio J_s/J increases from 1.0(2) to 27(4). At the same time, U/t is reduced (*20*), leading to an increase of the weak exchange J/h from 16(3) to 37(5) Hz. The inset shows the normalized spin correlator S quantifying the amount of antiferromagnetic ordering at the relevant density. Solid curves are the prediction of a high-temperature series expansion for an entropy-per-particle of $1.7k_B$ (as used in Fig. 3B) and are shown up to $t_s/k_BT = 1/2$. (**B**) Transverse spin correlator versus entropy before loading into the lattice at $U/t = 10.5(8)$ and $t_s/t = 7.3(6)$, together with a schematic view of the spin ordering. Error bars are as in Fig. 3.

closely resembles that of an explicit valence-bond solid (*3*).

To analyze the effect of temperature on the magnetic correlations, we measure the dependence of the singlet-triplet imbalance on the entropy in the harmonic trap s_{in} (Fig. 3A). The imbalance I and the absolute singlet fraction p_s reduce for larger entropies, as triplet states become thermally populated. The singlet fraction is additionally diminished by a shrinking half-filled region in the trapped system (*23*). We find good agreement with a second-order, high-temperature series expansion of coupled dimers when including an entropy increase of $\Delta s = 0.4k_B$, which is associated with the lattice loading (*24*); Δs is larger for the lowest entropies, consistent with previous results (*23*). From the measured imbalances we infer temperatures below $0.4J_d$, which corresponds to a trap-averaged entropy per particle of $1.6k_B$. Owing to entropy redistribution in the trap, the entropy per particle in the half-filled region drops below $0.6k_B$, which is 20% lower than for the isotropic simple cubic lattice [see (*20*)]. This reduction in entropy is even more pronounced for lower total entropies; in the absence of heating, this would result in entropies below $0.1k_B$ in the trap center.

For reduced dimerizations, the coupling between dimers leads to increased interdimer correlations. The excitation energy of triplets is then lowered as they delocalize over the lattice, thus changing the nature of magnetic ordering. In Fig. 3B, we use the tunable lattice to investigate the dependence of the imbalance I on the tunneling ratio t_d/t. In good agreement with theory, the imbalance decreases and eventually falls below our experimental resolution as the dimerization is progressively removed. This decrease can be attributed to the intradimer exchange energy J_d becoming smaller than the temperature T. For vanishing temperatures, the system is expected to undergo a quantum phase transition from a gapped spin-liquid state to a long-range–ordered antiferromagnet as t_d/t is reduced below a critical value, where the spin gap becomes zero (*2*, *25*). In the isotropic simple cubic lattice ($t_d/t = 1$), the system is in the metal–to–Mott insulator crossover regime with $U/t = 16(1)$ and a calculated hole probability of ~15% in the half-filled region (*20*).

The key to the observation of quantum magnetism in our system is the presence of two different exchange-energy scales. Without dimerization, this situation also occurs for anisotropic simple cubic lattices with tunneling t along two axes and a stronger tunneling t_s along the third direction. In this case, the symmetry between neighboring links is restored, and the detected singlet and triplet fractions are the same for both merging configurations. We observe a clear population difference $(p_s - p_{t_0})/2$ after loading a gas with entropies s_{in} below $1.0k_B$ into an anisotropic lattice, which increases to 4% for larger tunneling ratios t_s/t (Fig. 4A). The population difference is equal to the transverse spin correlator between neighboring sites i and $i + 1$ along the strong tunneling direction

$$-\langle S_i^x S_{i+1}^x\rangle - \langle S_i^y S_{i+1}^y\rangle = (p_s - p_{t_0})/2 \qquad (2)$$

Hence, this quantity directly characterizes the fraction of atoms with antiferromagnetic ordering on neighboring sites in the entire atomic cloud. Our observations also extend to weak lattices, where correction terms to the single-band Hubbard model become relevant (*26*). In this regime, a variety of magnetic phases have been predicted (*27*, *28*).

The results can be compared to a second-order, high-temperature series expansion (*20*). We find good agreement in the regime of small anisotropies. For larger anisotropies, the expansion breaks down as the strong tunneling and the temperature become comparable. In this regime, we expect the temperature to lie between the weak and strong exchange scales $J < k_BT < J_s$. The system then behaves as an array of 1D spin-ordered chains without correlations between them (*29*), where the majority of the entropy is stored in configurations involving the weak links. Low-dimensional systems have been predicted to show enhanced nearest-neighbor correlations (*30*).

For temperatures much larger than J_s, magnetic correlations should disappear. In Fig. 4B, we show the dependence on the initial entropy s_{in} and find the correlations to vanish above $2.5k_B$, where $k_BT >> J_s$ is expected.

Owing to the presence of the harmonic trap, most spin-correlated atoms are located in the center, where the filling is close to one particle per site. The density-normalized fraction of antiferromagnetic ordering is obtained when dividing by the fraction of atoms with two particles of arbitrary spin on adjacent sites. Under the assumption that all spin correlators $\langle S_i^{x,y,z} S_{i+1}^{x,y,z}\rangle$ are equal, which applies if all symmetry-breaking fields are much smaller than all other energy scales, the normalized spin correlator S can be directly obtained from the measurement of singlets and triplets (here, n_i^s is 1 for a single particle of any spin on site i and 0 otherwise)

$$S = \frac{-4\langle S_i^z S_{i+1}^z\rangle}{\langle n_i^s n_{i+1}^s\rangle} = \frac{p_s - p_{t_0}}{p_s + 3p_{t_0}} \qquad (3)$$

The normalized antiferromagnetic correlations along the strong tunneling direction reach 25% (Fig. 4A, inset), which corresponds to ~5000 ordered atoms.

Our local entropy redistribution scheme can be generalized to access the low-temperature regime in different geometries; for example, in weakly coupled 2D systems. Further extensions include the isolation of low-entropy regions via repulsive potentials, introducing additional lattice layers at different fillings as entropy reservoirs, or enhancing the tunnel coupling only in the central part of the atomic cloud. The tunable-geometry optical lattice allows the extension of our studies to spin-ladder systems, dimerized 1D chains, and zigzag chains, where the interplay between quantum fluctuations and magnetic ordering plays a particularly important role (*3*, *29*, *31*). At even lower temperatures, the existence of spin-liquids in honeycomb or triangular lattices could be investigated (*32*).

References and Notes

1. A. Auerbach, *Interacting Electrons and Quantum Magnetism* (Springer, New York, 1994).
2. S. Sachdev, *Nat. Phys.* **4**, 173 (2008).
3. H. T. Diep, G. Misguich, C. Lhuillier, in *Frustrated Spin Systems* (World Scientific, Singapore, 2005), pp. 229–306.
4. L. Balents, *Nature* **464**, 199 (2010).
5. P. W. Anderson *et al.*, *J. Phys. Condens. Matter* **16**, R755 (2004).
6. M. Lewenstein *et al.*, *Adv. Phys.* **56**, 243 (2007).
7. I. Bloch, J. Dalibard, W. Zwerger, *Rev. Mod. Phys.* **80**, 885 (2008).
8. T. Esslinger, *Annu. Rev. Condens. Matter Phys.* **1**, 129 (2010).
9. M. Köhl, H. Moritz, T. Stöferle, K. Günter, T. Esslinger, *Phys. Rev. Lett.* **94**, 080403 (2005).
10. R. Jördens, N. Strohmaier, K. Günter, H. Moritz, T. Esslinger, *Nature* **455**, 204 (2008).
11. U. Schneider *et al.*, *Science* **322**, 1520 (2008).
12. J. Simon *et al.*, *Nature* **472**, 307 (2011).
13. J. Struck *et al.*, *Science* **333**, 996 (2011).
14. S. Trotzky *et al.*, *Science* **319**, 295 (2008).
15. S. Nascimbène *et al.*, *Phys. Rev. Lett.* **108**, 205301 (2012).
16. T.-L. Ho, Q. Zhou, *Proc. Natl. Acad. Sci. U.S.A.* **106**, 6916 (2009).
17. J.-S. Bernier *et al.*, *Phys. Rev. A* **79**, 061601 (2009).
18. L. Tarruell, D. Greif, T. Uehlinger, G. Jotzu, T. Esslinger, *Nature* **483**, 302 (2012).
19. T. Uehlinger *et al.*, *Eur. Phys. J. Spec. Top.* **217**, 121 (2013).
20. See supplementary materials on *Science* Online.
21. S. Trotzky, Y.-A. Chen, U. Schnorrberger, P. Cheinet, I. Bloch, *Phys. Rev. Lett.* **105**, 265303 (2010).
22. S. Fuchs *et al.*, *Phys. Rev. Lett.* **106**, 030401 (2011).
23. D. Greif, L. Tarruell, T. Uehlinger, R. Jördens, T. Esslinger, *Phys. Rev. Lett.* **106**, 145302 (2011).
24. R. Jördens *et al.*, *Phys. Rev. Lett.* **104**, 180401 (2010).
25. Ch. Rüegg *et al.*, *Phys. Rev. Lett.* **93**, 257201 (2004).
26. F. Werner, O. Parcollet, A. Georges, S. R. Hassan, *Phys. Rev. Lett.* **95**, 056401 (2005).
27. C. J. M. Mathy, D. A. Huse, *Phys. Rev. A* **79**, 063412 (2009).
28. P. N. Ma, S. Pilati, M. Troyer, X. Dai, *Nat. Phys.* **8**, 601 (2012).
29. T. Giamarchi, *Quantum Physics in One Dimension* (Oxford Univ. Press, Oxford, 2003).
30. E. V. Gorelik *et al.*, *Phys. Rev. A* **85**, 061602 (2012).
31. P.-B. He, Q. Sun, P. Li, S.-Q. Shen, W. M. Liu, *Phys. Rev. A* **76**, 043618 (2007).
32. Z. Y. Meng, T. C. Lang, S. Wessel, F. F. Assaad, A. Muramatsu, *Nature* **464**, 847 (2010).

Acknowledgments: We thank N. Blümer, T. Giamarchi, C. Kollath, H. Moritz, C. Rüegg, M. Sigrist, N. Strohmaier, and S. Uchino for insightful discussions and U. Bissbort for help with the calculation of the Hubbard parameters in the dimerized lattice. We acknowledge the Swiss National Science Foundation, National Centre of Competence in Research–Quantum Science and Technology (QSIT), and Synthetic Quantum Many-Body Systems (European Research Council advanced grant) for funding.

Supplementary Materials

www.sciencemag.org/cgi/content/full/science.1236362/DC1
Materials and Methods
Supplementary Text
Figs. S1 to S6
References (*33*–*35*)

11 February 2013; accepted 7 May 2013
Published online 23 May 2013;
10.1126/science.1236362